Pergamon

Journal of Structural Geology, Vol. 19, No. 6, pp. 893 to 896, 1997

0191-8141/97 $17.00+0.00

PII: S0191-8141(97)00013-8

Brevia

SHORT NOTE

A velocity description of constant-thickness fault-propagation folding

STUART HARDY*

Institute of Earth Sciences (Jaume Almera), Consejo Superior de Investigaciones Cientificas (CSIC), Lluis Solé i Sabaris s/n, 08028 Barcelona, Spain

(*Received* 27 *August* 1996; *accepted in revised form* 15 *January* 1997)

Abstract—The expression of the geometric model of constant-thickness fault-propagation folding as a velocity description of deformation allows the derivation of rates of displacement, uplift and fault propagation. The velocity model of fault-propagation folding and sedimentation are combined in a finite-difference scheme, and two examples of growth strata associated with overturned fold forelimbs illustrate the application of the model. © 1997 Elsevier Science Ltd

INTRODUCTION

Since their introduction by Suppe and Medwedeff (1990) and Mitra (1990), the fixed-axis and constant-thickness fault-propagation fold models have been used extensively (e.g. Suppe *et al.*, 1992; Hardy and Poblet, 1995; Zapata and Allmendinger, 1996). In the fixed axial-surface model, thinning or thickening is allowed in the front limb of the fold while maintaining area. In the constant-thickness model, bed length and layer thickness are everywhere preserved. Constant-thickness folds have been suggest as being more common in the rock record (Suppe and Medwedeff, 1990). The constant-thickness theory allows overturned limbs, commonly seen in natural examples, to develop but the geometries of growth strata associated with such structures have only recently been investigated (Zapata and Allmendinger, 1996). Suppe and Medwedeff (1990) derived the basic equations of the constant thickness theory based upon the stratigraphic height (h) between the fault bend and the fault tip (Fig. 1). They went on to derive relationships between fault slip and front and backlimb length (Suppe *et al.*, 1992). However, for constant-thickness fault-propagation folds the backlimb length is only equal to the fault length when the step-up angle is 29°, a situation likely to occur in only a small fraction of natural examples. Therefore, there is no direct way of deriving the fault length for a given amount of slip and, thus, rates of fault propagation to fault slip for the majority of examples. In order to construct a velocity model of deformation, in which the rate and direction of displacement of material points are specified, such information is essential. It allows the definition of velocity domains, within which horizontal and vertical velocities are constant, as the fault accumulates slip (Fig. 1). Thus, rates of displacement within the structure and uplift above the structure can be derived. This Short Note presents a method for deriving such relationships without prior knowledge of stratigraphic height and derives a velocity model of constant-thickness fault-propagation folding. This velocity model of deformation can be combined with other rate-dependent processes, such as erosion, sediment transport and sedimentation, to model more realistic growth strata geometries than simple geometric models (e.g. Hardy and Poblet, 1995). Two examples of growth strata associated with constant-thickness fault-propagation folding illustrate the application of the model.

*Present address: Department of Geological and Geophysical Sciences, Guyot Hall, Princeton University, Princeton, NJ 08544,

CONSTANT-THICKNESS FAULT-PROPAGATION FOLDING

In order to define the geometry of a constant-thickness fault-propagation fold several steps must be undertaken.

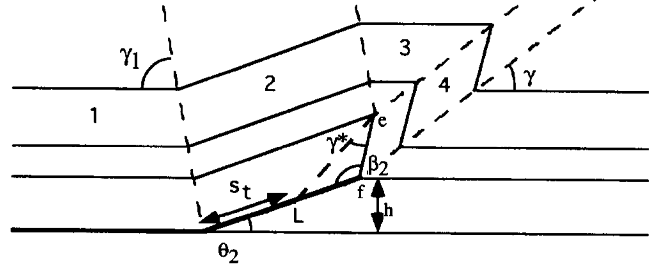

Fig. 1. The geometric model of constant-thickness fault-propagation folding of Suppe and Medwedeff (1990) with the controlling parameters illustrated for a ramp of 20° together with the four velocity domains.

First, one must solve the fundamental equation for simple-step constant-thickness fault-propagation folding (Fig. 1) with no external shear—equation (12) of Suppe and Medwedeff (1990):

$$\frac{1+2\cos^2\gamma^*}{\sin 2\gamma^*}+\frac{\cos\theta_2-2}{\sin\theta_2}=0 \tag{1}$$

which for a known value of θ_2 (the fault step-up angle) gives γ^*, the fold core interlimb angle. Knowing that

$$\gamma_1 = 90-\theta_2/2, \tag{2}$$

where γ_1 is the backlimb axial-surface angle, the front limb axial-surface angle, γ, can be then be found from

$$\gamma = 90+\gamma^*-\gamma_1. \tag{3}$$

Thus β_2, the angle between the fault and the front limb, is found from

$$\beta_2 = 180-2\gamma^*. \tag{4}$$

In contrast to geometric models, in which the configuration of the fold is found by working from a known value of h, we need to derive the length of the fault, L, the cutoff height, h, and the length between the fault tip and the anticlinal branching point, ef, for a given amount of slip s_t. The cutoff height, h, can be found from (rearranging equation 11 of Suppe *et al.*, 1992)

$$h=\frac{s_t}{\left[\dfrac{1}{\sin\theta_2}-\dfrac{1}{\sin(2\gamma-\theta_2)}\right]} \tag{5}$$

and the length, ef, is given by (simplifying equation 4 of Suppe and Medwedeff, 1990)

$$ef = h\left[\frac{1}{\sin(2\gamma^*)}\right]. \tag{6}$$

It is clear from Fig. 1 that the length of the fault, L, is given by

$$L = h/\sin(\theta_2). \tag{7}$$

combining equations (5) and (7) and simplifying, we obtain

$$L=\frac{s_t}{\left[1-\dfrac{\sin\theta_2}{\sin(2\gamma-\theta_2)}\right]}. \tag{8}$$

For a given step-up angle the relationship between the length of the fault and amount of slip is constant and needs only to be calculated once. The ratio of these values (fault length/fault slip) is equivalent to a fault propagation to slip ratio (Williams and Chapman, 1983). Ratios of fault propagation to fault slip for step-up angles in the range 10–50° are shown in Fig. 2. From this figure it can be seen that for step-up angles from 10° to 29° the ratio of fault propagation to fault slip increases approximately linearly from 1.55 to 2.0, whereas above this angle the ratio increases rapidly with step-up angle reaching a value of 5.25 at 50°.

Thus, for a given fault geometry and slip rate, the rate of fault propagation and the orientations of all active axial surfaces are known (Fig. 1). Velocities can now be derived for each of the domains shown in Fig. 1. It is important to note that there are four distinct velocity domains above the thrust, separated by active axial surfaces (Fig. 1). In domain 1 displacement is parallel to the lower décollement, in domain 2 displacement is parallel to the thrust ramp, and in domains 3 and 4 displacement is parallel to the leading active axial surface. The horizontal (u) and vertical (v) velocities in the four domains are then given by:

Domain 1
$$u = S \tag{9}$$
$$v = 0 \tag{10}$$

Domain 2
$$u = S\cos(\theta_2) \tag{11}$$
$$v = S\sin(\theta_2) \tag{12}$$

Domain 3
$$u = R_1\, S\cos(\gamma) \tag{13}$$
$$v = R_1\, S\sin(\gamma) \tag{14}$$

Domain 4
$$u = R_2\, S\cos(\gamma) \tag{15}$$
$$v = R_2\, S\sin(\gamma), \tag{16}$$

where S is the slip rate, θ_2 is the thrust ramp angle, R_1 and R_2 are changes in slip and γ is the inclination of the leading active axial surface. Between regions 1 and 2 there is no change in slip as the active axial surface is the bisector of the fault bend. However, between regions 2 and 3 and regions 2 and 4 there must be a change in slip across the velocity boundaries (active axial surfaces). The boundary between regions 2 and 4 runs along the line ef which connects the fault tip and the anticlinal branching point (Mosar and Suppe, 1992). The slip ratios between these regions (R_1 and R_2) are given by

$$R_1=\frac{\sin(\gamma_1+\gamma)}{\sin(\gamma_1+\theta_2)} \tag{17}$$

$$R_2=\frac{\sin(\beta_2-\theta_2+\gamma)}{\sin(\beta_2)} \tag{18}$$

following the approach given in Suppe *et al.* (1992).

GROWTH STRATA ASSOCIATED WITH CONSTANT-THICKNESS FAULT-PROPAGATION FOLDING

To illustrate the manner in which the velocity model described above may be used, two examples of growth

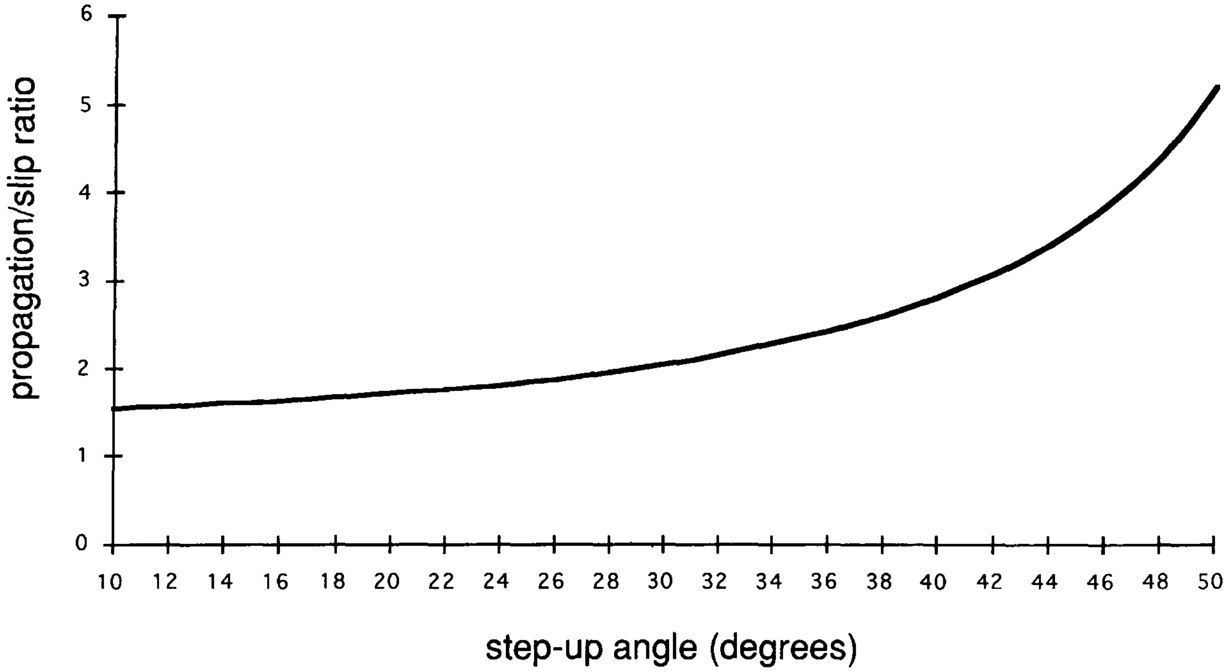

Fig. 2. The ratio of fault propagation to fault slip for simple-step constant-thickness fault-propagation folds for a range of values of step-up angle. Note that for higher step-up angles, a fault will propagate faster for a given amount of slip.

strata associated with constant-thickness fault-propagation folding are shown. The examples presented in this section have been modelled using a finite-difference approach described previously by Waltham and Hardy (1995). The tectonic deformation is modelled using the velocity description of deformation described above, while both background sedimentation and local erosion, transport and sedimentation are also modelled for the top surface in any two-dimensional numerical model. The methodology applied to compressional growth structures is described in detail in Hardy and Poblet (1995). A Eulerian finite-difference scheme is needed for the combination of tectonics and sedimentation for the topmost surface, while the deformation of buried surfaces is modelled using a simple Lagrangian scheme. This avoids any numerical diffusion or dispersion, and is particularly useful when steep or overturned surfaces are developed as a result of deformation (see Fletcher, 1991).

In the models described below sedimentation can be the result of two distinct processes: (1) background sedimentation; and (2) local erosion, transport and deposition. Background sedimentation is considered to be a non-locally sourced sedimentation rate, which occurs everywhere below a specified base level. Local erosion, transport and sedimentation are modelled in the example where uplift exceeds burial using a diffusion mechanism in which sediment flux is proportional to local slope. The diffusion model results in material being eroded and transported away from any steep slopes which develop during a model run. Mathematical details are given in Hardy and Poblet (1995).

In both examples a step-up angle of 20° is used with a slip rate of 1 m/ka over a total run time of 1 Ma. Growth strata are recorded at intervals of 200 ka. In the first example only background sedimentation is modelled, with background sedimentation occurring at a rate of 1 m/ka which is greater than the uplift at the crest of the fold (Fig. 3a). It can be seen that this example possesses an overturned forelimb in both pre-growth and growth strata, and a series of complex growth axial surfaces. This is particularly marked on the forelimb and crest of the structure, where the kinematics are quite complex. For low step-up angles, such as this example, material rolls onto the crest of the structure producing the complex relationships observed. A more realistic model is presented in Fig. 3(b), where all model parameters are identical except that the base level rise and background sedimentation rate are both reduced to 0.4 m/ka and a diffusion coefficient of 1.0 m^2/a is used to simulate local erosion, transport and sedimentation. This is a situation commonly observed in many fault-related folds where structures uplift faster than the local sedimentation rate and form a topographic high (cf. Zapata and Allmendinger, 1996). The value of the diffusion coefficient appears to depend on a variety of factors such as climate, lithology and scale (Kooi and Beaumont, 1994). The value used here was chosen because it illustrates well the distinctive features caused by the interaction of tectonics and sedimentation in this setting. Note the deep erosion on the crest and backlimb of the structure, and the onlap of growth strata onto this erosion surface. Also worth noting is the difficulty in distinguishing between growth and pre-growth strata on the forelimb of the structure, as

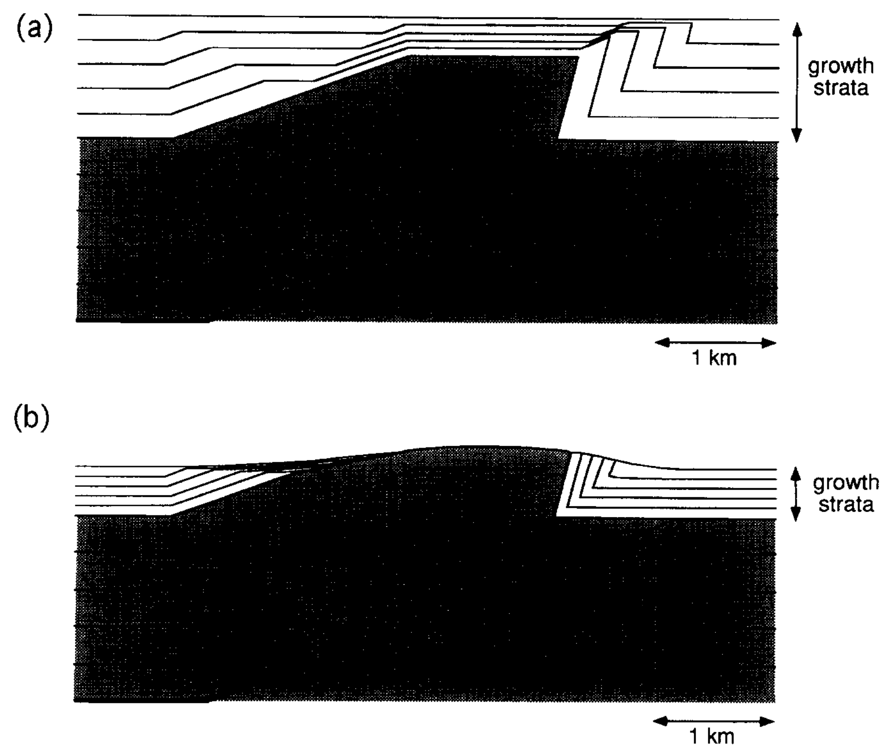

Fig. 3. Examples of growth strata associated with constant-thickness fault-propagation folding: (a) base level rise and sedimentation greater than uplift rate above the structure; and (b) base level rise less than uplift rate above the structure together with a diffusion model of erosion, transport and sedimentation. No vertical exaggeration. Model parameters are given in the text.

this is now a region of uplift and erosion and the strata do not interact with an active axial surface on the crest of the structure.

CONCLUSIONS

This Short Note has derived a velocity description of constant-thickness fault-propagation folding and a simple expression relating fault propagation to fault slip. The power of this approach is that it is consistent with previous geometric approaches but also allows rates of fault propagation and uplift to be derived given an external slip rate. The derived velocities can then be used in simple mathematical models to test the geometric consequences of such kinematics within both growth and pre-growth strata (cf. Hardy and Poblet, 1995). The inverse problem, determining rates of fault propagation and fault slip, can also be approached if geometric and age constraints are available for a given structure.

Acknowledgements—Thanks to Tomás Zapata for sparking my interest in this topic in a manuscript review, and to Josep Poblet, Mary Ford and Dave Waltham for many fruitful discussions. Comments made by Wes Wallace and an anonymous reviewer considerably helped to improve this note. The receipt of a Royal Society European Science Exchange Post Doctoral Fellowship is gratefully acknowledged. A copy of the modelling program for Power Macintosh computers is available from the author upon receipt of a diskette.

REFERENCES

Fletcher, C. A. J. (1991) *Computational Techniques for Fluid Dynamics. Volume 1, Fundamentals and General Techniques*, 2nd ed. Springer, New York.
Hardy, S. and Poblet, J. (1995) The velocity description of deformation. Paper 2: sediment geometries associated with fault-bend and fault-propagation folds. *Marine and Petroleum Geology* **12**, 165–176.
Kooi, H. and Beaumont, C. (1994) Escarpment evolution on high-elevation rifted margins: Insights from a surface process model that combines diffusion, advection, and reaction. *Journal of Geophysical Research* **99**(B6), 12191–12209.
Mitra, S. (1990) Fault-propagation folds: geometry, kinematic evolution ad hydrocarbon traps. *Bulletin of the American Association of Petroleum Geologists* **74**, 921–945.
Mosar, J. and Suppe, J. (1992) Role of shear in fault-propagation folding. In *Thrust Tectonics*, ed. K. R. McClay, pp. 123–137. Chapman and Hall, London.
Suppe, J. and Medwedeff, D. A. (1990) Geometry and kinematics of fault-propagation folding. *Eclogae Geologicae Helvetiae* **83**, 409–454.
Suppe, J., Chou, G. T. and Hook, S. C. (1992) Rates of folding and faulting determined from growth strata. In *Thrust Tectonics*, ed. K. R. McClay, pp. 105–121. Chapman and Hall, London.
Waltham, D. and Hardy, S. (1995) The velocity description of deformation. Paper 1: Theory. *Marine and Petroleum Geology* **12**, 153–163.
Williams, G. and Chapman, T. (1983) Strains developed in the hanging-walls of thrusts due to their slip/propagation rate: a dislocation model. *Journal of Structural Geology* **5**, 563–571.
Zapata, T. R. and Allmendinger, R. W. (1996) Growth strata records of instantaneous and progressive limb rotation in the Precordillera thrust belt and Bermejo basin, Argentina. *Tectonics* **15**, 1065–1083.